

Small scale impact on rigid barrier using transparent debris-flow models

Nicoletta Sanvitale^{a,*}, Elisabeth Bowman^a, Miguel Angel Cabrera^b

^aUniversity of Sheffield, Sir Frederick Mappin Building, Mappin St., Sheffield, S1 3JD, UK

^bUniversidad de los Andes, Carrera 1 Este No. 19^a-40, Bogotá, 111711, Colombia

Abstract

Fast landslides, such as debris flows, involve high speed downslope motion of rocks, soil and water. Their high flow velocity, high degree of runout and potential for impact make them one of the most hazardous gravitational mass flows. While the estimation of the pressure generated by the impact of debris flows on civil engineering structures has been widely investigated, the state of the knowledge is still insufficient to accurately describe the dynamics and load evolution of the impact process. Both fluid and solid forces influence the dynamics of debris flows but existing design approaches for barrier or mitigation structures tend to treat these geophysical flows as a single continuum, neglecting the solid fluid-interactions. Hence in the literature, impact models are yet largely semi-empirical. This paper presents the first results of experiments using transparent debris flows in a small-scale flume aiming at investigating the mechanism of impact on rigid barriers. The use of a transparent debris-flow model allows the movements of particles and fluid within the medium to be probed. We examine flows consisting of uniform and well graded particle size gradings at two different fluid contents. The evolution of the impact load, bed normal pressure and fluid pore pressure for the different flows are measured and analysed in order to gain a quantitative comparison of their behaviour before and after impact.

Keywords: Debris flows; Barriers; Physical modelling; Transparent soil

1. Introduction

A debris flow is a rapid surging flow of saturated-debris and soil in a steep channel that may present high impact load and long runout (Iverson, 1997; Takahashi, 2007; Hungr et al., 2013). A common method to prevent these flows from reaching vulnerable areas is by obstructing their channelized paths with barriers, dampening the overall flow inertia, trapping most of the transported debris, and, therefore, decreasing their expected runout. These barriers can be rigid walls or flexible nets, with a main goal of withstanding the impact forces from the transported debris and suspended material.

Rigid barriers, also called catch dams, are the most common mitigation structure against debris flows, due to the minimal technical skills required in their construction and easiness in the supply of building materials for reinforced concrete. These barriers sustain the lateral impact forces by self-weight, consisting of a debris-flow breaking structure, a retention basin and a pre-structure (Hübl et al., 2009). While the estimation of the pressure generated by the impact of debris flows on civil engineering structures has been widely investigated (Moriguci et al., 2009, Armanini et al., 2011; Bugnion et al., 2011; Hu et al., 2011; Scheidl et al, 2012; Cui et al., 2015; Zhou et al., 2018.), the state of knowledge is still insufficient to accurately describe the dynamics and load evolution of the impact process.

The current paper presents the first results of experiments using transparent analogue debris flows in a small-scale flume, aiming at investigating the bulk impact forces on rigid barriers. The experimental variables are the initial particle size distribution and fluid content while measuring the impact forces against the obstacle, the basal total- and fluid-pressures, flow height, and the cross-sectional flow dynamics at impact observed via Planar Laser Induced Fluorescence, PLIF (Sanvitale & Bowman, 2012). Section 2 presents details on the experimental setup and its

* Corresponding author e-mail address: n.sanvitale@sheffield.ac.uk

instrumentation, describing the materials employed and experimental protocol. Section 3 focuses on the direct measurements and discusses the impact mechanisms. Finally, Section 4 presents the main conclusions of the current work and provides insights into ongoing research.

2. Methods

2.1. Experimental set up

The material is stored in a rectangular tank, at the top of the channel. A slice gate, fitted between acrylic seals, releases the material by hand pull. The material flows down a rectangular flume 2.57 m long and 0.15 m wide, at an adjustable angle (see Fig. 1). Experiments reported in this paper are performed for a flume inclination of 20°. The lateral walls are made of borosilicate glass and the flume's bottom is roughened with 3D-printed PLA plates with a hexagonal packing of 3 mm semi-spheres. The roughened bed is instrumented along its base with three pore pressure transducers, PPT2, 3 and 4 (PDCR 810 Druck) placed at 175 mm centres along the flume at 30 mm from the centerline with PPT2 placed closest to the barrier at 8.5cm distance and PPT3 and PPT4 placed 175mm and 350mm further upslope. One load cell (LUX-B-ID Kyowa) with a circular sensing plate of 23mm diameter is mounted flush with the flume across from PPT2 (at 30 mm on the other side of the centerline). All basal sensors have 3D printed disk headings, equivalent to the roughness of the rest of the base.

The barrier model is made of a PMMA plate 10 mm thick, 150 mm wide and 190 mm tall (Fig. 1). The plate is connected to an aluminum support, connected at one end, on its mid-width, to an axial load cell (U9C, HBM) and fixed on its base to a linear bearing (LZMHS12-37T2P1, SKF). The barrier model is fixed to the flume bed at 2.25 m from the gate release, and is orientated normal to the flow direction (see inset in Fig. 1).

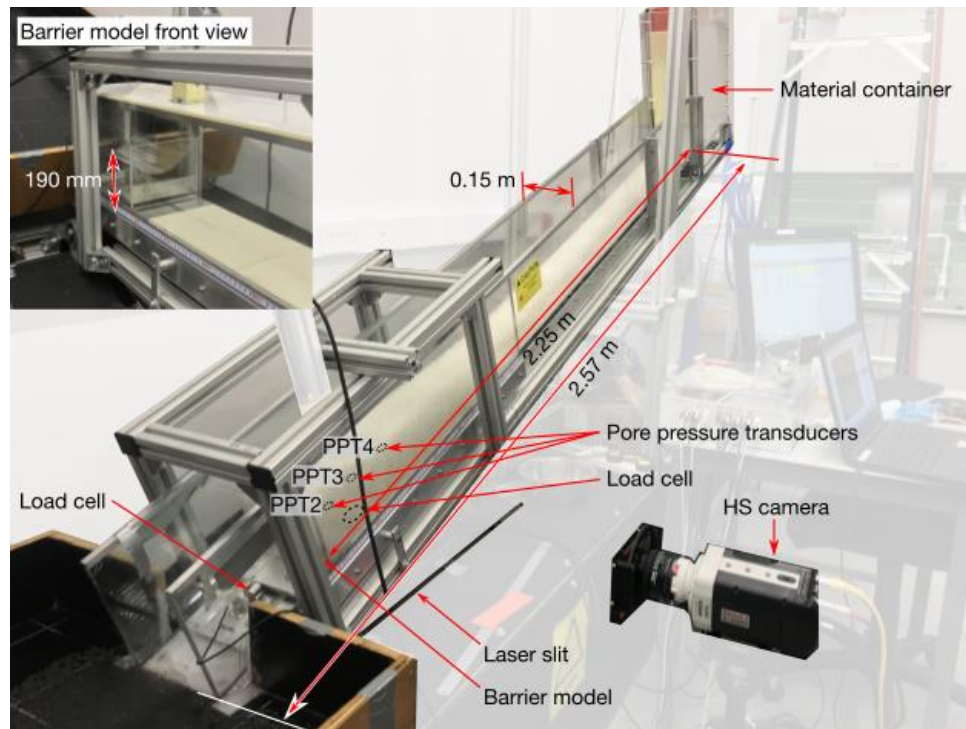


Fig. 1. Experimental setup after test. (Inset) Barrier model front view.

A 0.5 mm thick 532 nm laser light sheet is allowed to pass through the roughened bed and barrier model base, illuminating the flowing material at the flume's mid-width. The illuminated plane is located about in front of the barrier lighting the material from the flume's bottom (Fig. 1). The longitudinal motion is recorded with a Phantom high speed camera at a frame rate of 2000 fps. For more details on the PLIF technique please refer to Sanvitale and Bowman (2012).

2.2. Materials

In order for the PLIF technique to work under optimum conditions, the fluid and solid should present a match of their refractive indices. The current experiments are performed with hydrocarbon oil (Cargille laboratories) dyed with a fluorescent powder, and mixed with borosilicate glass beads (Sigmund Lindner GmbH). The fluid has a viscosity that is higher than water and a density that is lower, such that particle / fluid consolidation behaviour is equivalent to that using quartz particles that are four times smaller in water (Sanvitale & Bowman, 2012). Three particle size distributions (PSD) are employed in experiments; two uniform samples with glass beads of 3 mm and 7.5 mm, and a well graded sample (coefficient of uniformity $C_U=6$) with mean particle size of 7.5 mm (see Fig. 2). These samples are intended to provide an insight on the potential effects of particle size distribution on the impact mechanism.

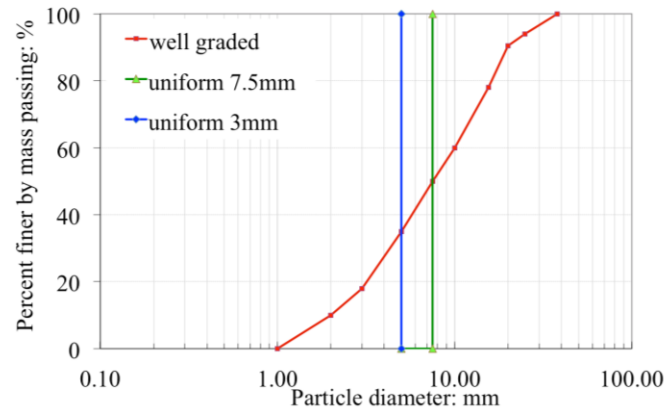


Fig. 2. Glass beads samples particle size distribution.

2.3. Test procedure

Experiments explore the effects of 28% and 32% fluid content f_c , defined as $\text{mass}_{\text{fluid}}/\text{mass}_{\text{solid}}$, impacting a rigid barrier model. Prior to experiment, the flume is cleaned, avoiding the presence of oil films on the roughened bed and lateral walls. For each experiment 10 kg of glass beads are used. Oil is gently poured into the container and mixed with the glass beads, paying special attention to the removal of air bubbles inside the mixture. Once the desired amount of fluid is added into the container, the laser beam is set-on, the high-speed camera is activated, and the slice gate is opened. At release, a triggering shutter connected to the gate activates the sensor recording at a sampling rate of 36 kHz, for a duration of 9 s.

3. Results and discussion

Qualitative features of flow impact can be revealed by the analysis of the video images. Figure 3 presents a sequence of images for each PSD at the fluid content, f_c 28% (images for f_c 32% are not shown for brevity). Fig. 4 shows the runup height at the barrier measured on the video footage for all the tests except the well graded flow with 32% of fluid content, for which the movie was not available. The images show different instants during the impact of the mixture against the barrier with respect to the time $t=0$ at which the slice gate was opened. Images on the left column show the initial phase of the impact, the middle image is taken when the runup of the material occurs and the image on the right shows the final phase of each test. All the tests displayed similar dynamics during the impact, with preliminary collisions of dry bouncing particles against the barrier prior the arrival of the flow front. Only in the test with 3mm beads and f_c 28% could we observe the arrival of a first small frontal surge before the impact of the main flow surge.

The impact of the leading surge led to a runup that exceeded for a few centimeters the height of the barrier for all the experiments except for the 3mm mixture at f_c 28% (Figure 4). However during runup only a small quantity of mixture was able to override the barrier because the vertical wave produced rapidly broke backward, resulting in an upstreaming propagating shock wave. The same behavior was observed by Iverson et al. (2016) in large scale flume tests using soil and water mixtures.

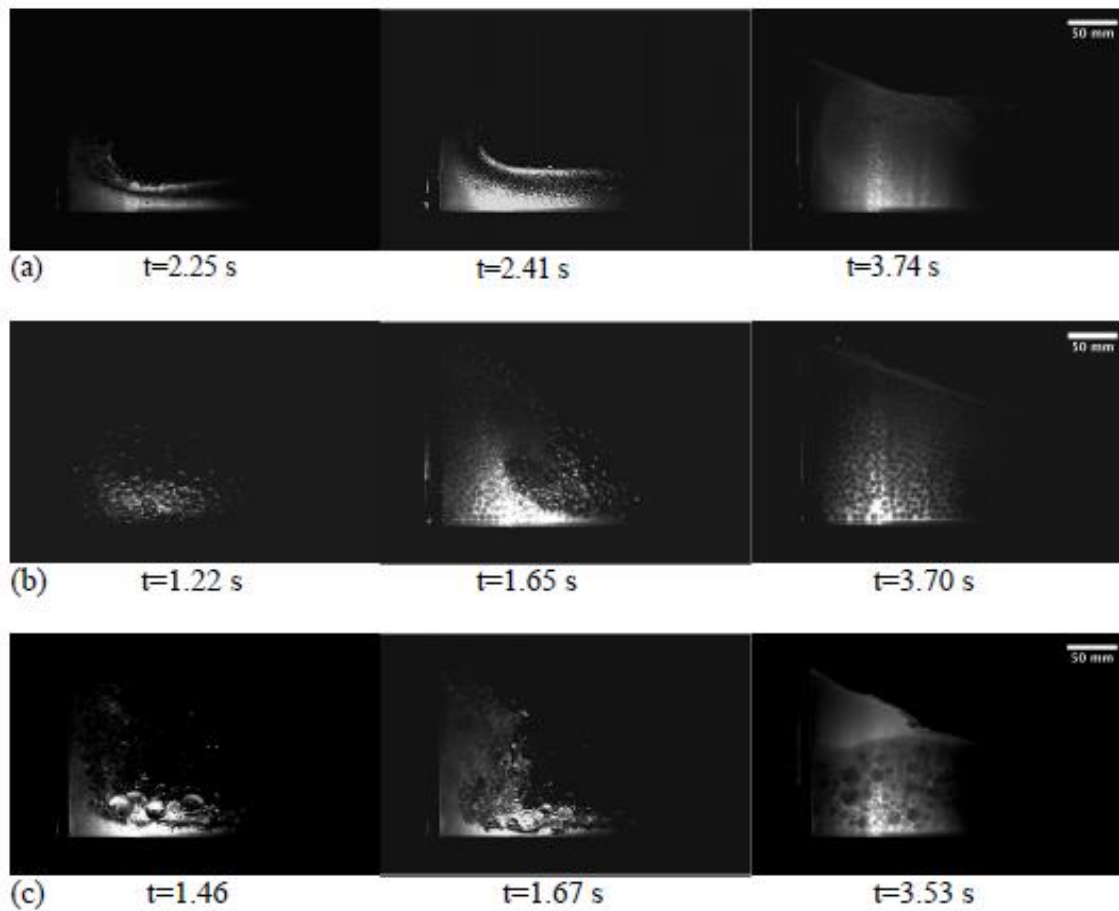


Fig. 3. Illuminated section at centerline of flume during impact (a) 3mm uniform, (b) 7.5mm uniform, (c) well-graded with $D_{50} = 7.5\text{mm}$, $C_U = 6$

The velocity of the tests is generally larger at higher fluid content. The front velocity of the tests at f_c 28%, estimated using the instant at which the flow front arrive at the barrier, is approximately 1.1 m/s, 1.9 m/s and 1.8 m/s \pm 0.2 m/s for the 3mm, 7.5mm and well graded PSDs, respectively. When the fluid content is 32% the estimated front velocity is 1.6m/s, 2.1m/s, 1.9 m/s \pm 0.2 m/s for the 3mm, 7.5mm and well graded PSDs, respectively. The estimate of the instant in which the flow arrives at the barrier is not an easy task due to the fact that the tests are run in a dark environment to avoid any light except that produced by the fluorescent dye excited by the laser being recorded by the high speed camera. As the flow front is usually unsaturated, we can only track the position of the flow front from the reflected light coming from the reflections of the laser with the surface of the beads. Further work is ongoing to obtain the field velocity during impact using particle image velocimetry analyses on the flow images.

3.1. Basal pressure development

Figs 5 and 6 shows the responses of the pore pressure transducers using a running filtering window of 300 Hz. The PPT responses are dominated by the increase in the height of the fluid-saturated debris behind the barrier (which is effectively impermeable) after impact. Therefore, although flows initially pass over PPT4, then PPT3 and then PPT2 in succession on their descent (resulting in relatively small recorded pressures of the order of 0.2 kPa), PPT2 (closest to the barrier) then produces the largest and earliest response to this impact with recorded pressures ranging between 1 and 2 kPa.

There is a considerable difference in pore pressure behaviour after impact between flows at f_c 28% and 32%, particularly for the 3mm flows which, considering the ratio of pore pressure to total stress, appears to be close to hydrostatic for f_c 28% but above this immediately post impact for f_c 32%. For the well graded flows, it is clear that the

pore pressures are much greater than hydrostatic upon and post impact at both fluid contents. For the 7.5mm flows, the picture is mixed – appearing slightly above hydrostatic for the 28% and considerably above for f_c 32%. These results point to several things: excess pore pressures do not necessarily generate within uniform flows of spheres, except where sufficient fluid is present and sufficient agitation is generated (e.g. during an impact event).

The 7.5 mm flows generate large forces at impact, higher velocities and greater agitation than the 3mm flows, although otherwise it would be expected from consolidation theory the finer material should both generate and maintain higher pore pressure. This only occurs for the 3mm flow at f_c 32%, showing that the fluid content plays a role in developing excess pore pressure which is necessary for enhanced mobility. Conversely, for well-graded flows (at least for the chosen grading and same fluid contents) excess pore pressures are both generated and maintained at impact. This is likely due to there being both larger particles to agitate the flow upon impact and fines to reduce permeability and hence maintain the excess pore pressure for longer.

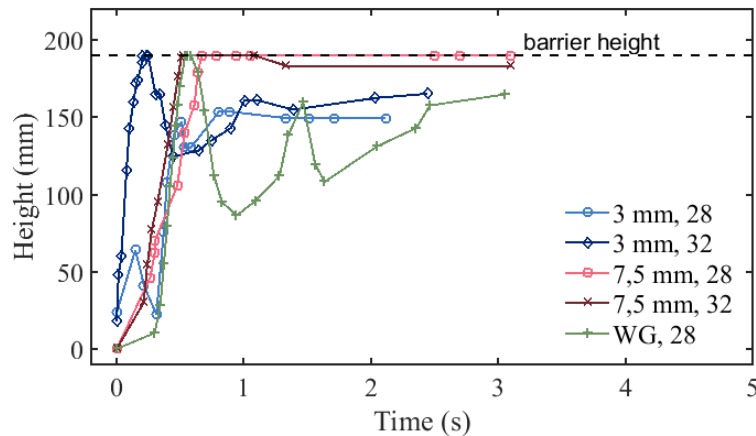


Fig. 4. Measured run-up height at the barrier (time $t=0$ is the time of the flow front arrival)

3.2. Impact load

The recorded raw impact signals present high frequency spikes that can be due to random effects depending on the resonance frequency of the load cell and on single instantaneous impact of large particles. In order to filter the data we followed the procedure proposed by Scheidl et al. (2012), applying a low pass filter with a maximum high frequency estimated considering the average maximum front velocity v_f and the maximum particle diameter, as follows $f_i = v_f / d_{max}$. For the uniform tests with 3 mm and 7.5 mm particles this produced a low pass frequency of 450 Hz and 270 Hz respectively. For the well graded material we decided to assume as d_{max} the value of $d_{90} = 20$ mm and obtained a low pass frequency of 100 Hz.

Figures 5 and 6 present the impact load measured during tests after filtering. The influence of the particle size on the response of the barrier is clear. The uniform flows with the 7.5 mm particles generate the greatest initial impact load, while that of the well graded flow (with d_{50} of 7.5 mm and d_{90} of 20 mm) is intermediate to that of the 3 mm and 7.5 mm for both fluid content series.

The well graded tests such as those with 7.5 mm show a number of spikes in the impact signal recorded from the load cell, representing collisions of large particles against the barrier, however, both the peak force during and after the impact reach values similar to those of 3 mm mixtures. This indicates the dampening influence of the fine particles within this flow material, considering that it has larger particles than the uniform 7.5 mm flows.

Comparing the videos with the development of the impact load it is possible to recognize common dynamics for all the tests. We observe an initial dynamic impact characterized by the rapid increase of the load due to the front surge arrival and the subsequent material runup hitting the barrier. The impact force peak is followed by a quick drop when the runup wave breaks backward down, suppressing the action of the incoming flow for a subsequent runup. From this point on, the increase of the impact force can be considered as a result of the progressive deposition of the mixture behind the material already settled in front of the barrier.

The peak load due to the initial dynamic impact of the flows appears to be enhanced by the presence of a larger quantity of fluid for the 7.5 mm and well graded tests. The 3 mm tests do not show a greater initial impact at larger fluid content but instead it is possible to observe a slight increase in the load exerted from the flow after the impact,

probably due to the fact that the more fluidised mixture results in a faster flow and hence most of the particles within the mixture are able to travel till the end of the channel, increasing the weight of the material behind the barrier (see Fig. 4).

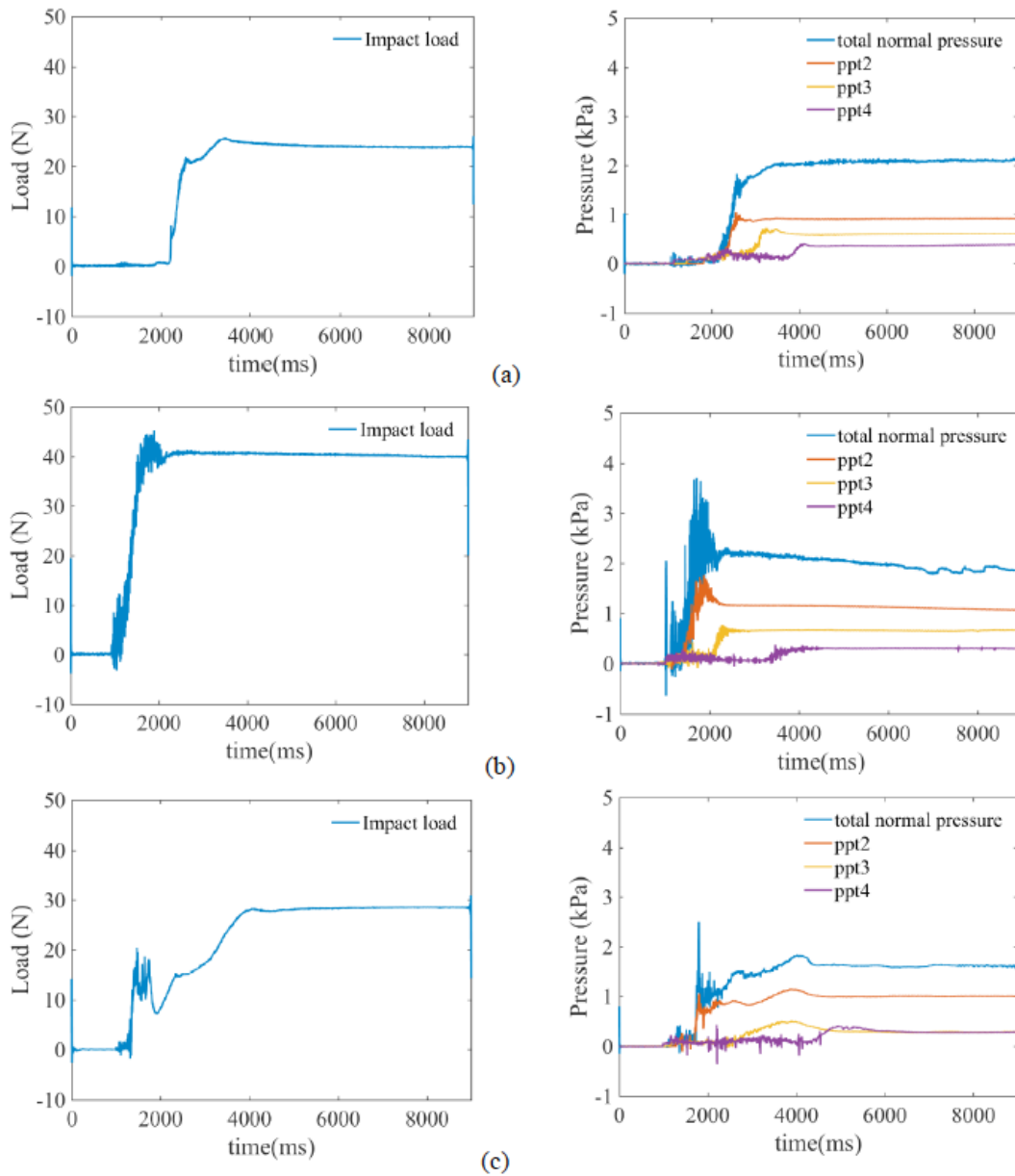


Fig. 5. Fluid content 28% (Left) Load on barrier (Right) Basal pressures (a) 3mm uniform, (b) 7.5mm uniform, (c) well-graded with $D_{50} = 7.5\text{mm}$, $C_u = 6$

Closer examination shows that the flow at f_c 28% for the 3 mm particles behaves similarly to that of the 7.5 mm flows with a near constant pressure response after impact, however at f_c 32%, it is more similar to that of the well graded flows where the impact pressure initially rises then falls then rises again. Coupled with the pore pressure response for 3 mm, this suggests that the behaviour of this uniform flow strongly depends on the fluid content.

Only the 7.5mm tests exhibited a peak load generated by the initial dynamic impact on the barrier that is higher than that exerted from the material deposited behind. The reason for that is that such fast mixtures, once they hit the

barrier, can produce a high and large runup wave with large particles that, despite their size, can be easily mobilized and pushed upward and against the barrier exerting high pressure.

In contrast, it is clearly visible from the high speed camera video, that for the f_c 28% well graded test, most of the top part of the runup wave is comprised of fluid as the large particles at the flow front are too heavy to be pushed any higher than approximately the middle height of the barrier (Fig. 3). Furthermore, the presence of finer material can also have a damping effect on the large particle collisions. The combination of these factors can explain the similar value of the impact load between the 3 mm and the well graded tests.

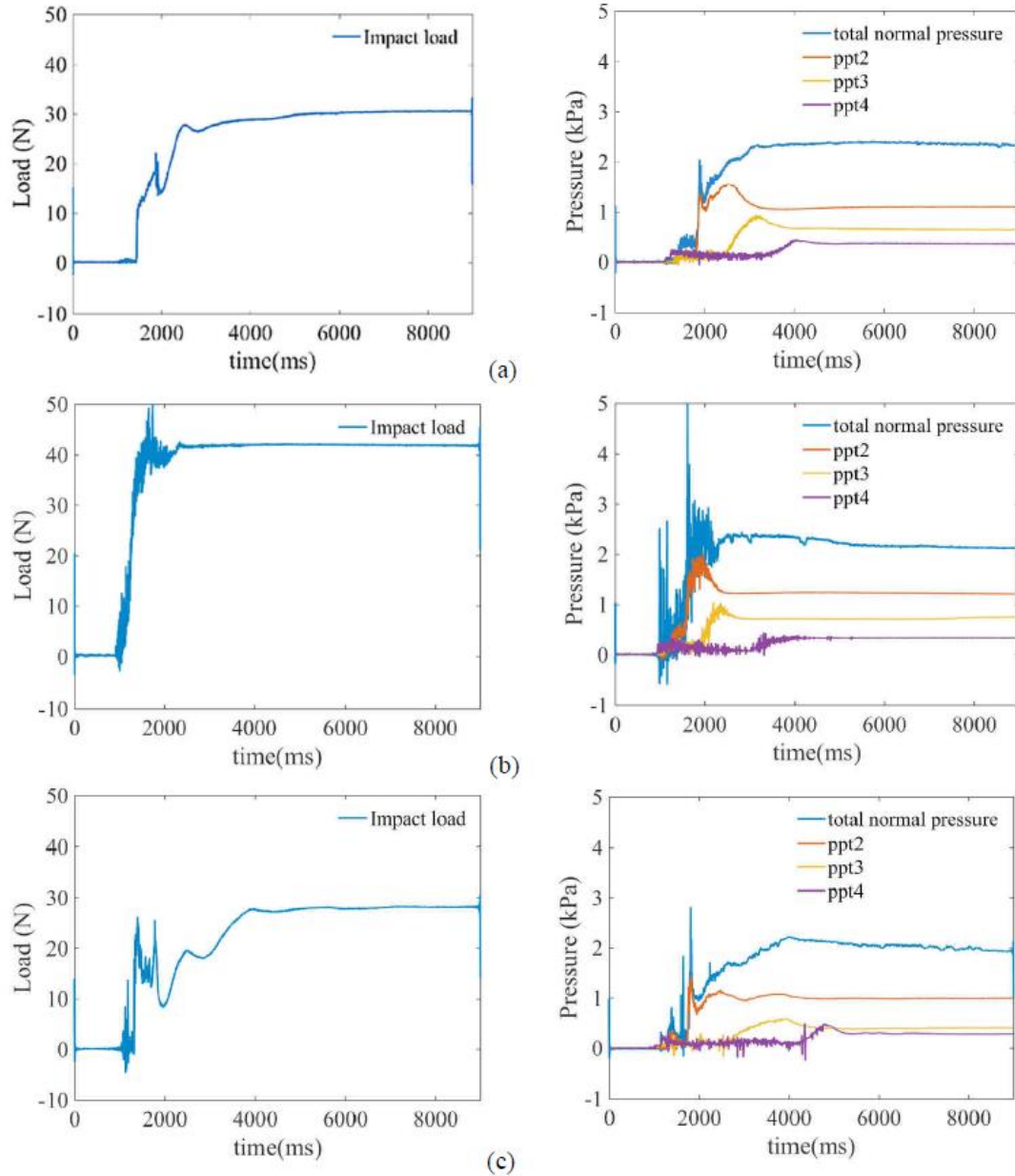


Fig. 6. Fluid content 32% - (Left) Load on barrier (Right); Basal pressures (a) 3mm uniform, (b) 7.5mm uniform, (c) well-graded with D_{50} 7.5mm, $C_U = 6$

4. Conclusions

The paper presents the results of tests performed using a small-scale flume in which the impact of a transparent debris-flow model on rigid barrier is investigated. The roughened base of the channel is instrumented along its base with three pore pressure transducers and a load cell for the measure of the total normal stress. The barrier is fixed to the flume bed at 2.25 m from the gate release and is orientated normal to the flow direction.

The evolution of the impact load, bed normal pressure and fluid pore pressure for flows consisting of uniform and well graded particle size gradings at two different fluid contents, 28% and 32%, is measured and analyzed before and after impact. It has been found that excess of pore pressures do not necessarily generate within uniform flows of spheres, except where sufficient fluid is present and sufficient agitation is generated (e.g. during an impact event). The particle size of the material has an effect on impact. The uniform flows with the larger particles generate the greatest initial impact load while for the well graded mixture the presence of fine particles within the flow can provide a dampening influence. Further work is ongoing to obtain the field velocity during impact using particle image velocimetry analysis on the flow images in order to investigate the impact kinematics in detail.

Acknowledgements

This research was supported through the Engineering and Physical Sciences Research Council (EPSRC), UK project no. EP/M017427/1 “High speed granular debris flows: new paradigms and interactions in geomechanics”. The authors would like to acknowledge the assistance of technicians at the University of Sheffield in the construction of the apparatus. MAC was partly funded by the Early-stage Researcher fund (FAPA) from the Universidad de los Andes, under the Grant agreement No. PR.3.2016.3667.

References

- Armanini, A., Larcher, M., and Odorizzi, M., 2011, Dynamic impact of a debris flow front against a vertical wall, in Proceedings, 5th international conference on debris-flow hazards, .Mitigation, mechanics, prediction and assessment, Padua, p. 1041–1049.
- Bugnon, L., McArdell, B., Bartelt, P., and Wendeler, C., 2011, Measurements of hillslope debris-flow impact pressure on obstacles: Landslides, p. 1–9, doi:10.1007/s10346-011-0294-4.
- Cui, P., Zeng, C., and Lei, Y., 2015, Experimental analysis on the impact force of viscous debris flow: Earth Surf. Processes Landforms, v.40, p. 1644–1655, doi:10.1002/esp.3744.
- Hu, K., Wei, F., and Li, Y., 2011, Real-time measurement and preliminary analysis of debris-flow impact force at jiangjia ravine, china: Earth Surf Process Landf., v. 36, p. 1268–1278, doi:10.1002/esp.2155 .
- Hubl, J., Suda, J., Proske, D., Kaitna, R., and Scheidl, C., 2009, Debris-flow impact estimation, in Proceedings of the 11th International Symposium on Water Management and Hydraulic Engineering, Ohrid, Macedonia.
- Hungr, O., Leroueil, S., and Picarelli, L., 2013, The Varnes classification of landslide types, an update: Landslides, v. 11, p. 167-194.
- Iverson, R.M., 1997, The physics of debris flows: Reviews of Geophysics, v. 35, no. 3, p. 245-296.
- Iverson, R.M., George, D.L., and Logan, M., 2016, Debris-flow run-up on vertical barriers and adverse slopes: Journal of Geophysical Research-Earth Surface, v. 121, p. 2333–2357, doi:10.1002/2016JF003933.
- Moriguchi, S., Borja, R., Yashima, A., and Sawada, K., 2009, Estimating the impact force generated by granular flow on a rigid obstruction: Acta Geotech., v. 4, no. 1, p. 57–71.
- Sanvitale, N., and Bowman, E.T., 2012, Internal imaging of saturated granular free-surface flows: International Journal of Physical Modelling in Geotechnics, v. 12, no. 4, p. 129-142.
- Scheidl, C., Chiari, M., Kaitna, R., Mullegger, M., Krawtschuk, A., Zimmermann, T. and Proske, D., 2012, Analysing debris-flow impact models, based on a small scale modelling approach: Surveys in Geophysics, v. 34, no. 1, 121–40.
- Takahashi, T. 2007. Debris flow: Mechanics, prediction and countermeasures. Taylor & Francis.
- Zhou, G.G.D., Song, D., Choi, C.E., Pasuto, A., Sun, Q.C., and Dai, D.F., 2018, Surge impact behavior of granular flows: effects of water content: Landslides, v. 15, no. 4, p. 695-709.